Embedded Piezoelectric Sensing for Metallic Components: A Novel SHM Architecture for Self-Aware Structures

PEIYUAN ZHOU, JINHAN REN, JAMES S. SCHURE,
SHINAN HUANG, SAZEDUR RAHMAN, SANDIPAN MISHRA,
JOHNSON SAMUEL, SEMIH AKIN
and FOTIS KOPSAFTOPOULOS

ABSTRACT

This study presents a novel structural health monitoring (SHM) architecture for self-aware structures based on hybrid manufacturing for fabricating multifunctional metallic components with subsurface-embedded piezoelectric (PZT) sensors, enabling autonomous SHM capabilities. The developed methodology integrates Wire Arc Additive Manufacturing (WAAM), subtractive machining, and Cold Spray Additive Manufacturing (CSAM) to seamlessly embed commercial off-the-shelf PZT sensors within aluminum structures (Al-5356) while preserving structural integrity. The embedded sensors are protected by ceramic thermal barriers and metallized surfaces, facilitating process resumption for complex geometries. The experimental validation is based on acousto-ultrasonic guided wave (GW) propagation analysis under controlled mechanical loading (0-100 MPa) and thermal cycling (ambient to 100^{o}C). Active-sensing configurations utilizing pitch-catch methodologies demonstrate equivalent performance to surface-mounted sensors, with capacitance-based electromechanical impedance signatures confirming sensor functionality. The fabricated self-sensing structures exhibit real-time diagnostic capabilities for detecting operational (static load) and environmental (temperature) state changes, demonstrating particular advantages for applications where surface-mounted sensors are impractical due to coating requirements or environmental protection constraints. This hybrid manufacturing framework establishes a foundation for next-generation intelligent metallic structures with integrated SHM functionality.

INTRODUCTION

Structural health monitoring (SHM) methodologies have evolved significantly across diverse engineering applications, transitioning from periodic inspection protocols to continuous real-time assessment frameworks for detecting structural degradation throughout operational lifecycles. However, conventional SHM architectures predominantly rely on externally mounted sensor arrays, which exhibit fundamental limitations under harsh environmental conditions and demonstrate reduced sensitivity for detecting subsurface

Fotis Kopsaftopoulos, Associate Professor, Intelligent Structural Systems Lab (ISSL), Department of Mechanical, Aerospace and Nuclear Engineering, Rensselaer Polytechnic Institute, Troy, NY, USA; Email: kopsaf@rpi.edu

damage initiation during early-stage failure progression [1–3]. These constraints become particularly important in applications involving high-temperature exposure, corrosive environments, or surface coating requirements that preclude external sensor mounting.

The paradigm of "self-aware structures" addresses these technological gaps by integrating sensing capabilities directly within structural components through advanced manufacturing techniques, enabling autonomous condition assessment without external sensor dependencies [4]. This approach facilitates the development of intelligent structural systems capable of real-time health monitoring while maintaining structural performance characteristics and operational reliability. Among various embedded sensing modalities, piezoelectric transducers, particularly lead zirconate titanate (PZT) elements, demonstrate exceptional capabilities for advanced SHM applications due to their inherent dual-functionality as both actuators and sensors [5]. PZT-based systems offer several distinct advantages: (i) high electromechanical coupling efficiency enabling bidirectional energy conversion between mechanical strain and electrical signals for in-situ monitoring applications [6]; (ii) enhanced environmental sensitivity for detecting operational parameter variations including temperature fluctuations and mechanical loading conditions [7]; and (iii) compact form factors with minimal weight penalties, facilitating integration into load-bearing metallic structures without compromising structural integrity [8]. When positioned within critical structural regions, embedded PZT sensors enable continuous monitoring of dynamic structural response characteristics, providing autonomous damage detection capabilities through guided wave propagation analysis [3,9]. Despite significant technological promise, seamless integration of PZT sensors within metallic components presents substantial manufacturing challenges, particularly regarding preservation of host structure mechanical properties and sensor protection under operational conditions.

Current embedded sensor integration approaches face critical limitations in achieving robust sensor protection while maintaining manufacturing process continuity for complex geometries. Furthermore, most embedded sensor fabrication techniques cannot accommodate process resumption for additive manufacturing operations, limiting their applicability to simple geometric configurations. Therefore, this investigation presents a novel hybrid manufacturing framework that systematically addresses these limitations through the development self-aware metallic structures with subsurface-embedded commercial off-the-shelf (COTS) PZT sensors. The methodology integrates Wire Arc Additive Manufacturing (WAAM), precision subtractive machining, and Cold Spray Additive Manufacturing (CSAM) to achieve seamless sensor integration while preserving both structural performance and sensor functionality.

The fabricated self-aware structures undergo comprehensive experimental validation through controlled mechanical loading protocols (0-100 MPa stress range) and thermal cycling assessments (ambient to 100^{o}C temperature range) to quantify sensor performance under representative operational conditions. Active-sensing configurations utilizing pitch-catch guided wave methodologies enable systematic evaluation of sensor responsiveness and diagnostic capability. Non-parametric signal analysis techniques provide quantitative assessment of structural state awareness capabilities, with particular emphasis on stress-dependent and temperature-dependent signal characteristics. This research establishes a foundation for next-generation intelligent metallic structures with integrated SHM functionality, demonstrating particular advantages for applications where

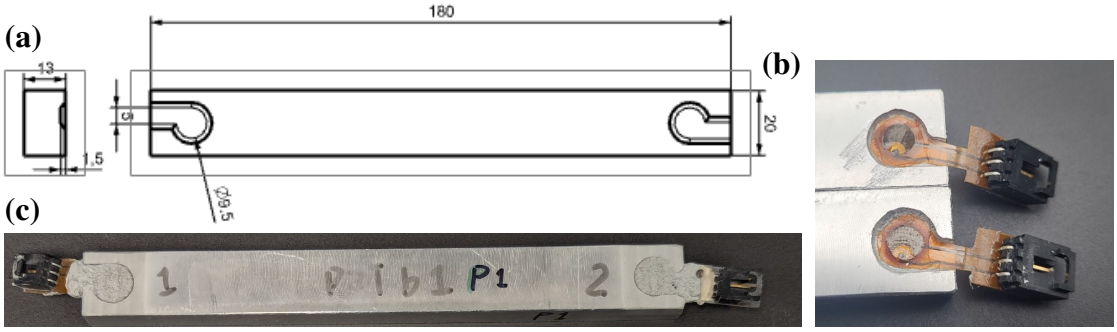

Figure 1. (a) Design of the self-aware structures with subsurface embedded sensors; (b) COTS PZT sensors bonded within the sub-surface cavities of the beam; (c) Representative image of the fabricated beam with embedded PZTs.

conventional surface-mounted sensors are impractical due to environmental constraints, coating requirements, or geometric limitations.

FABRICATION OF SELF-AWARE STRUCTURES

The self-aware structural system integrates two commercial off-the-shelf piezoelectric transducers (Acellent Technologies, SMLSSOP4NR) through a novel hybrid manufacturing approach combining additive, subtractive, and surface modification processes, as shown in Figure 1a. The fabrication methodology implements five sequential stages:

1. Wire Arc Additive Manufacturing: Host beam fabrication using Al-5356 alloy
2. Precision machining: Subsurface sensor cavity formation
3. Sensor integration: Adhesive bonding within machined cavities
4. Ceramic protection: Thermal barrier deposition for environmental shielding
5. Surface metallization: Cold Spray Additive Manufacturing (CSAM) for process continuity

The host beam structure (180 mm $\times$ 20 mm $\times$ 13 mm) is fabricated using Al-5356 alloy WAAM with Cold Metal Transfer (CMT) welding technology, enabling controlled material deposition at reduced thermal input. A 6-axis robotic manipulator (Yaskawa) executes the layered deposition strategy with 20 sequential weld beads and 6 mm hatch spacing, as detailed in the sensor-integrated manufacturing cell [10]. Critical process parameters are systematically controlled per Table 1 specifications. Sensor housing cavities are precision-machined 1.5 mm below the upper surface using CNC operations with a 3.175 mm ball end mill (Figure 1a-b). Controlled spindle speed (4,000 rpm) and feed rate (50.8 mm/min) minimize thermal effects while achieving required surface finish. PZT transducers are integrated using high-performance epoxy adhesive (Loctite EA9394 Aero), selected for superior temperature resistance and mechanical properties under dynamic loading.

A ceramic thermal barrier is deposited over the sensor assembly, providing protection against high-temperature exposure, oxidation, and moisture infiltration while eliminating stress concentrations. Surface metallization utilizes CSAM technology, which is a low-temperature process capable of producing dense metallic coatings without melting the feedstock powders [11]. CSAM is used to deposit aluminum-rich powder feedstock onto the surface of the ceramic layer, creating a homogeneous metal surface. The corresponding CSAM parameters are provided in Table 1. The integrated hybrid manufacturing framework demonstrates flexibility through systematic process control and

validation protocols, ensuring dimensional accuracy, optimal material properties, and preserved sensor operational capabilities throughout the fabrication sequence.

EXPERIMENTAL EVALUATION

The fabricated self-aware structure undergoes systematic performance assessment through three controlled experimental protocols: (i) static loading evaluation; (ii) quasi-static loading assessment; and (iii) transient thermal characterization. Guided wave (GW) signals are acquired synchronously with corresponding environmental and operational conditions (EOC) to quantify sensor responsiveness and diagnostic capabilities. Signal variations are analyzed relative to stress and temperature parameters using established damage identification (DI) methodologies.

Static and Quasi-Static Loading Evaluation

The sample beam is subjected to three-point-bending configuration for the static and quasi-static loading tests with maximum stress calculated as:

$$\sigma_f = 3PL/2bd^2, \tag{1}$$

where the support length L is 120 mm, the beam width b is 20 mm, and the beam depth d is 13 mm. The universal test machine controls stress based on load cell feedback, integrated with a NI PXIe 6393 data acquisition system for synchronized stress-GW measurements (sampling rate of 3.3 MS/s; Figure 2a). The universal test machine is integrated with the NI PXIe data acquisition system as illustrated in Figure 2a, where an

Table 1. Fabrication parameters for the self-aware metal structure.

Fabrication Process	**Parameter**	**Value (unit)**
Step-1 WAAM	Material	Aluminum (Al-5356)
	Wire feed rate	400 inch/min ($\sim$ 0.17 m/s)
	Torch speed	4 mm/sec
	Number of weld beads	20
	Beads (hatch) distance	6 mm
Step-2 Machining	Cutting tool	3.175 mm ball end mill
	Spindle speed	4,000 rpm
	Feed rate	2 inch/min ($\sim$ 50.8 mm/min)
Step-3 Surface metallization	Material	Mixture of Al, Al_2O_3, and Zn
	Gas temperature	400 °C
	Gas pressure	6 bar (0.6 MPa)
	Nozzle transverse speed	20 mm/sec
	Nozzle stand-off distance	25 mm

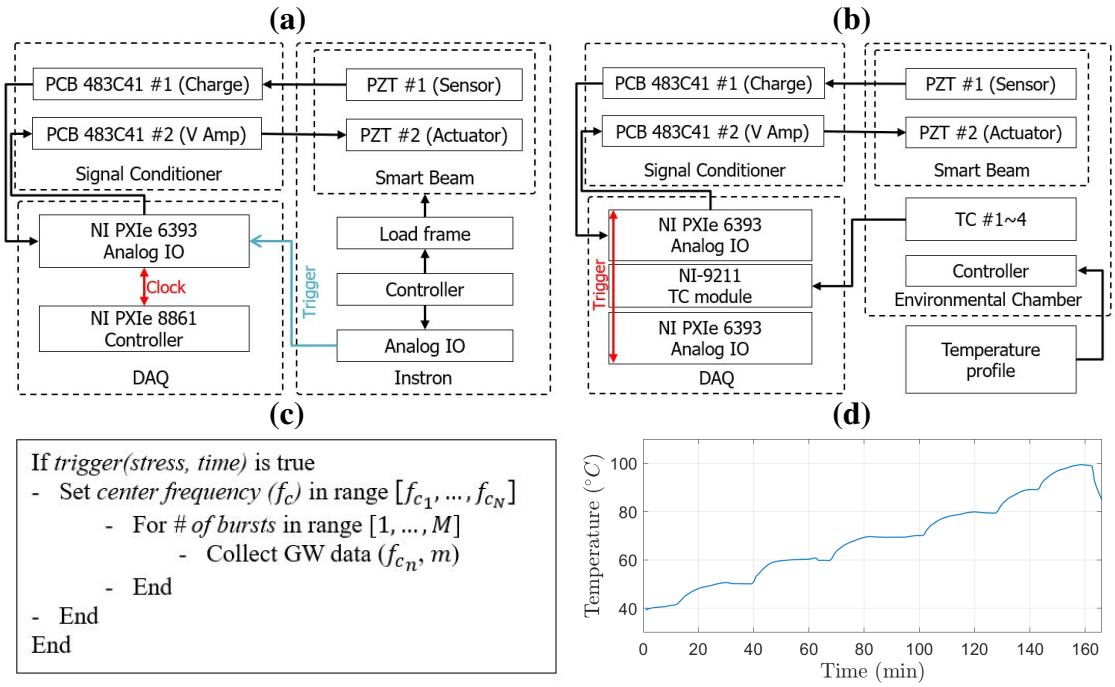

Figure 2. (a) GW data under quasi-static load is acquired using PXIe system synchronized with the Instron universal test machine that acquires corresponding load condition. (b) GW data collection under varying temperature uses an additional TC module synchronized to the GW acquisition task.

analog output is used to trigger the acquisition of GW data. Actuation signals are 5-peak tone bursts (5-cycle Hanning-filtered sine wave) generated at several center frequencies ($f_c = \{100 : 50 : 500\}$ kHz) and amplified from 0.4 V_{p-p} to 16 V_{p-p} using a signal conditioner (*PCB 483C41*) in voltage mode. Then, the response of the other PZT is conditioned and amplified by another *483C41* module in charge mode. In the static loading case, multiple data sets were collected per center frequency, while the stress was kept constant. In the quasi-static loading case, while quasi-static testing implements stress ramping from 1-100 MPa at 1 MPa/min with data collection at 3 MPa increments. Figure 2c shows the detailed data acquisition process, and the experimental parameters are shown in Table 2.

Transient Thermal Evaluation

In the transient thermal test, the beam was subjected to an arbitrary increasing tem-

Table 2. Summary of experimental details.

Test	**Trigger event**	**Center frequency (f_c)**	**Burst per f_c**
Static	$\sigma_f = \{0 : 10 : 100\}$ MPa	$\{100 : 50 : 500\}\ kHz$	40
Quasi-static	$\sigma_f = \{1 : 3 : 99\}$ MPa	$\{100 : 50 : 500\}\ kHz$	20
Thermal	$\Delta t = 50\ s$	$\{100 : 50 : 500\}\ kHz$	40

perature profile in an environmental chamber. The actual chamber temperature is measured by 4 type-E thermocouples and the average is plotted in Figure 2d. In order to accurately associate environmental temperature with GW data for subsequent analysis, temperature measurement on NI-9211 and GW measurement on PXIe-6396 were synchronized by a 0.020 Hz external counter output from another manually controlled PXIe-6396 module. When a GW acquisition subroutine is triggered, similarly, a number of GW bursts and responses were acquired for each center frequency as the temperature varies with the corresponding temperature value.

Reference Literature DIs

In the non-parametric analysis of acquired GW data, three different DIs are employed to evaluate the potential of the PZT-embedded beam in the SHM application. First, Janapati et al. [12] proposed a DI that is sensitive to damage size and orientation and agnostic to material property variation, which is formulated as:

$$Y_u^n[t] = \frac{y_u[t]}{\sqrt{\sum_{t=1}^{N} y_u^2[t]}}, \quad Y_0^n[t] = \frac{\sum_{t=1}^{N} \left(y_0[t] \cdot Y_u^n[t]\right)}{y_0[t] \cdot \sum_{t=1}^{N} y_0^2[t]}, \quad DI = \sum_{t=1}^{N} \left(Y_u^n[t] - Y_0^n[t]\right) \tag{2}$$

Baseline signal $y_0[t]$ and unknown signal $y_u[t]$ are discrete time series data with $t = 1, 2, 3, ..., N$. $Y_0^n[t]$ and $Y_u^n[T]$ are normalized baseline and unknown signals. The Qiu correlation-based approach focuses on waveform and time-of-flight variations:

$$DI = 1 - \sqrt{\frac{\left(\sum_{t=1}^{N} y_0[t] \cdot y_u[t]\right)^2}{\sum_{t=1}^{N} y_0^2[t] \cdot \sum_{t=1}^{N} y_u^2[t]}} \tag{3}$$

The third DI is the standard root mean square deviation (RMSD) that quantifies the difference between a baseline and an unknown signal:

$$DI = \sqrt{\frac{\sum_{t=1}^{N} (y_0[t] - y_u[t])^2}{\sum_{t=1}^{N} y_0^2[t]}} \tag{4}$$

RESULTS AND ANALYSIS

Acquired GW response data was preprocessed including mean removal and statistical averaging across repetitive acquisitions at identical trigger conditions. The temporal averaging process leverages the quasi-static nature of environmental and operational condition (EOC) evolution relative to GW acquisition timeframes, yielding enhanced signal-to-noise ratios and reduced stochastic variability. Statistical mean calculations utilize 40 repetitive responses per center frequency for static/thermal tests and 20 responses for quasi-static evaluations, as detailed in Table 2. The average signals are plotted in Figures 3-5, and their respective close-ups of indicative wave packs influenced by stress and temperature.

Under static loading conditions, signal evolution demonstrates clear stress-dependent characteristics. Time-of-flight reduction is observed in representative signals (Figure 3(a.2, b.2), corresponding to compressive deformation effects at the sensor embedment locations. Signal amplitude attenuation correlates with increasing stress levels, attributed

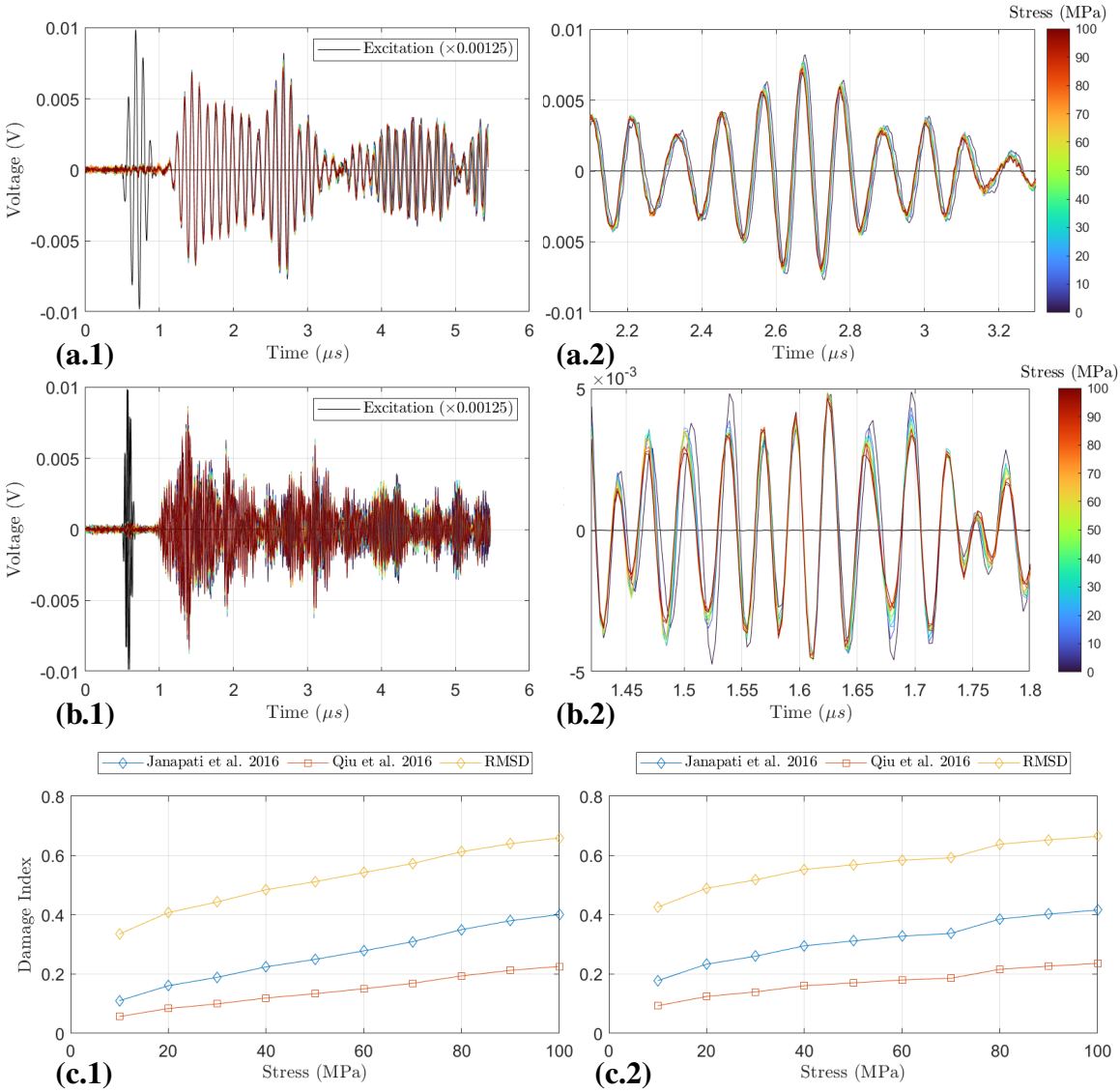

Figure 3. Indicative GW signals beam for increasing static load, from 0 Mpa to 100 MPa with 10 MPa increment, at two different center frequencies: a) 100 kHz, and b) 300 kHz. Close up of GW signals are shown, respectively, in (a.2) and (b.2). DIs are plotted for GW signals at each stress level for (c.1) 100 kHz and (c.2) 300 kHz.

to combined effects of stress distribution variations and modified boundary conditions throughout the loading sequence. All three DI formulations exhibit distinctive correlations with applied stress variations. All DIs demonstrate monotonic sensitivity to stress increments, while the Qiu correlation-based approach shows enhanced discrimination capabilities at intermediate stress levels. Similar performance is observed at both center frequencies.

Quasi-static loading reveals similar GW signal variations with enhanced temporal resolution across the stress progression (Figure 4(a.2, b.2)). The increased sampling density provides detailed DI evolution trends compared to static loading assessments. Nonlinear DI progressions are systematically observed across all center frequencies, indicating complex stress-wave interaction mechanisms within the embedded sensor configuration. The 100 kHz and 200 kHz excitation frequencies demonstrate distinct sensitivity

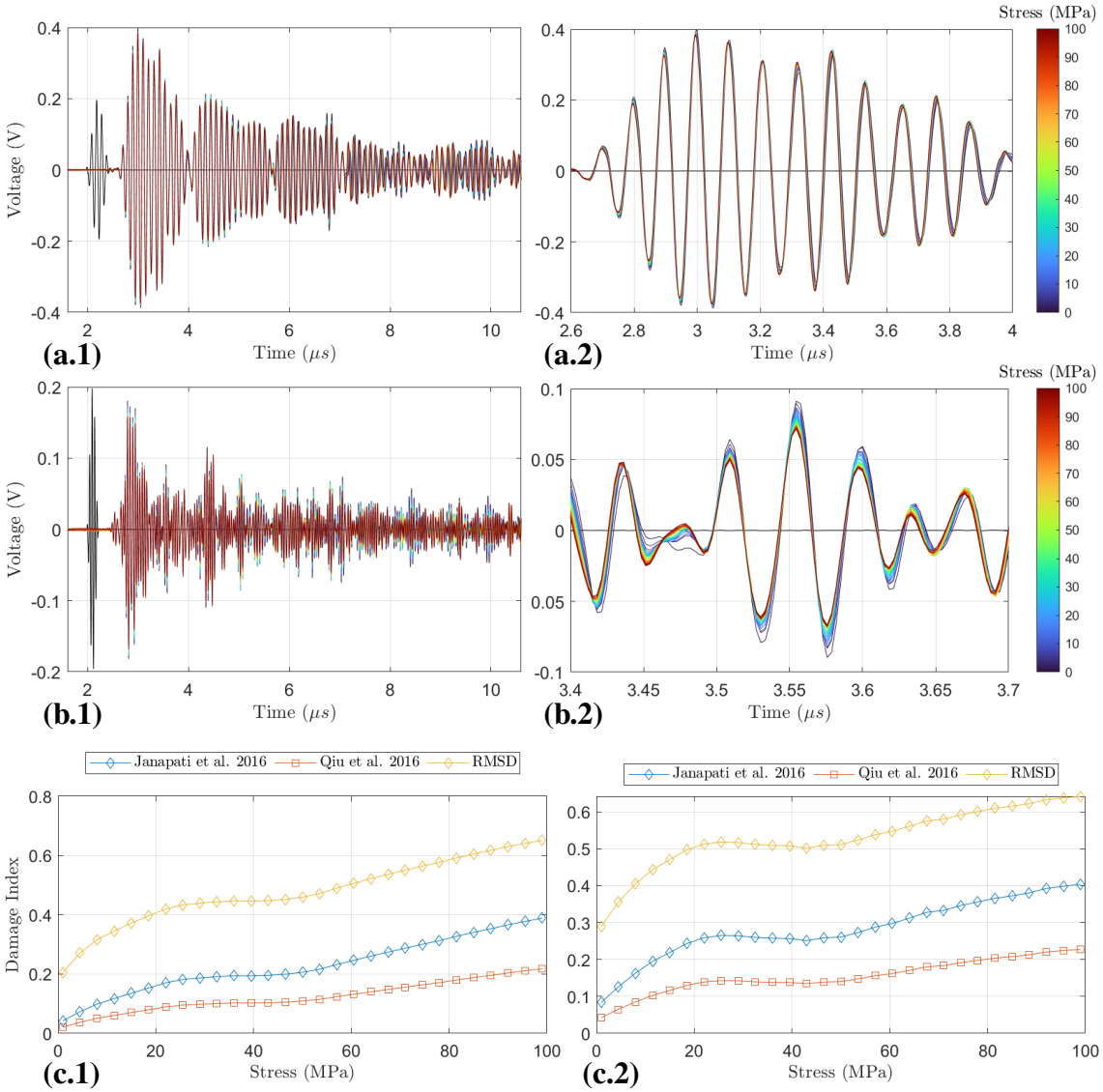

Figure 4. Indicative GW signals for increasing quasi-static load from 0 MPa to 100 MPa at two different center frequencies: a) 100 kHz and b) 200 kHz. Close up of GW signals are shown, respectively, in (a.2) and (b.2). DIs are plotted for GW signals with respect to stress level for (c.1) 100 kHz and (c.2) 200 kHz.

profiles, with 200 kHz signals exhibiting higher DI values. This frequency-dependent behavior suggests optimal sensor interrogation strategies for specific operational stress ranges, enabling adaptive monitoring protocols based on anticipated loading conditions.

Thermal characterization reveals complex sensor response patterns under controlled temperature cycling from 70 °C to 100 °C. Significant amplitude reduction is observed across all frequency ranges (Figure 5(a.2, b.2)), with time-of-flight and wave packet characteristics exhibiting nonlinear temperature dependencies. These variations result from combined effects of material property changes, thermal expansion coefficients, and temperature-dependent adhesive bonding characteristics. DI evolution during thermal cycling demonstrates frequency-specific behaviors requiring systematic analysis. The 100 kHz DI exhibits reverse trend regions between 70-80 °C, while the RMSD saturates above 80 °C, indicating threshold-limited sensitivity ranges. Conversely, 200 kHz exci-

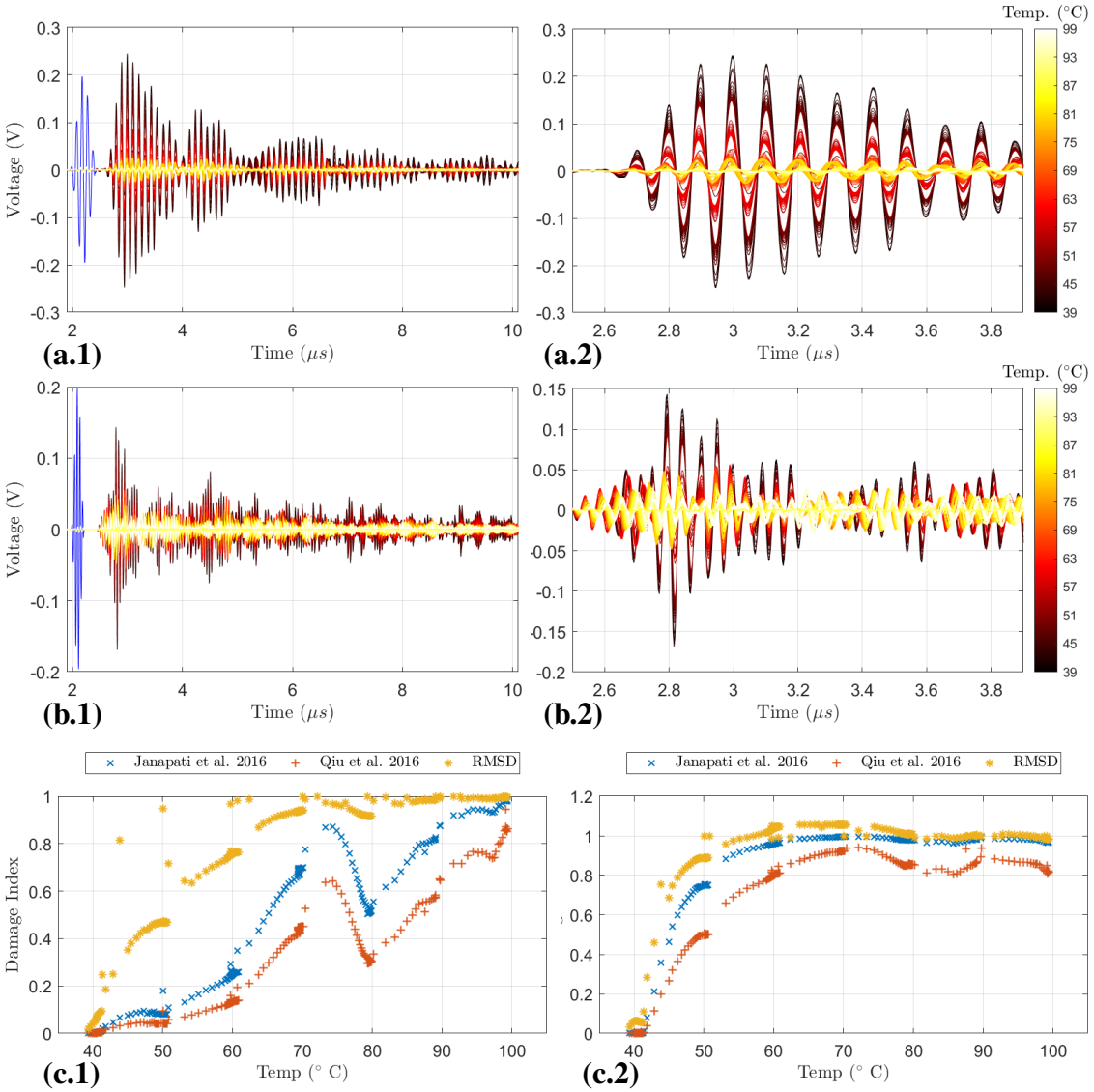

Figure 5. Indicative GW signals under ramp-and-hold thermal input at two different center frequencies: a) 100 kHz and b) 200 kHz. Close up of signals shown, respectively, in (a.2) and (b.2). DIs plotted at each temperature for (c.1) 100 kHz and (c.2) 200 kHz.

tation shows earlier saturation onset (around 60 °C) with distinct reverse region characteristics from 70-100 °C, suggesting complex thermomechanical coupling effects within the sensor-structure interface.

DISCUSSION

The experimental assessments encompassing static/quasi-static loading and transient thermal characterization demonstrate the structural state awareness capabilities achieved through the PZT-embedded beam architecture. Comparative analysis of nonparametric signal characteristics and established DI formulations confirm that embedded PZT sensors maintain equivalent electromechanical performance to surface-mounted configurations. The placement flexibility of PZT sensors across material thickness, enabled through the proposed additive manufacturing approach, facilitates future optimization

protocols for controlled excitation of selective guided wave modal characteristics.

Notably, the metallization step over the ceramic shielding during the fabrication stage (Figure 1c) holds strong potential for fabricating functional interlayers that could be compatible with various AM processes (e.g., WAAM, laser-directed energy deposition, laser powder bed fusion). This feature can facilitate the seamless resumption of the AM processes on the sensor-integrated beam, which might potentially pave the way for large-scale smart metallic structures. It is particularly important, as many AM techniques face challenges in achieving strong and conformal interlayers to ensure reliable bonding and structural continuity during process resumption. As such, the proposed hybrid manufacturing pathway can effectively address the relevant limitations of conventional approaches, while preserving the interfacial integrity between the host structure and the subsequently deposited layers.

Despite these promising results, the smart beam exhibited a moderate reduction in both stiffness and strength compared to baseline beams. This mechanical debit is likely attributed to the presence of the machined sensor cavities, which act as stress concentrators within the structure. However, it should be noted that the mechanical debit data was obtained from a single specimen (i.e., single data point) and therefore requires further investigation through repeating testing and statistical analysis to ensure reproducibility and reliability. To enhance the mechanical debit, the following strategies may be considered: (i) sensor network topology refinement; (ii) simulation-assisted thermal and stress field estimation utilizing reduced sensor density; and (iii) manufacturing process enhancement to minimize stress concentration effects from machined cavities.

CONCLUDING REMARKS

In this study, we presented a "Self-aware" Beam with subsurface-embedded PZT sensors, fabricated by a novel hybrid manufacturing approach. In a host structure built by wire-arc additive manufacturing (WAAM), PZT elements were placed in subtractive machined cavities and then fully encapsulated by a subsequent cold-spray AM process under the protection of ceramic fillings. The following conclusion can be drawn from the present study that the embedded PZT elements are capable of operating in the "pitch-catch" configuration to function as the foundation of active sensing SHM. GW signals showed variations correlated to the evolution of stress and temperature. Additionally, referenced DIs showed results comparable to literature applications.

In summary, this study validated the developed Smart Beam and its hybrid manufacturing approach as a promising framework for advanced SHM applications. These efforts can open new aveneus for designing and development of intelligent, multifunctional metal structures. Future work will focus on expanding the sensing modalities and assessing the long-term durability of the Smart Beams under dynamic and cyclic loading conditions to support field-ready implementation.

ACKNOWLEDGMENT

This work was performed under agreement (# HR00112490367) between the Defense Advanced Research Projects Agency (DARPA) and Rensselaer Polytechnic Institute (RPI). Internal funding from RPI is also acknowledged.

REFERENCES

1. Lehmhus, D., C. Aumund-Kopp, F. Petzoldt, D. Godlinski, A. Haberkorn, V. Zöllmer, and M. Busse. 2016. "Customized Smartness: A Survey on Links between Additive Manufacturing and Sensor Integration," *Procedia Technology*, 26:284–301, ISSN 2212-0173, doi:https://doi.org/10.1016/j.protcy.2016.08.038, 3rd International Conference on System-Integrated Intelligence: New Challenges for Product and Production Engineering.
2. Salowitz, N., Z. Guo, S. Roy, R. Nardari, Y.-H. Li, S.-J. Kim, F. Kopsaftopoulos, and F.-K. Chang. 2014. "Recent advancements and vision toward stretchable bio-inspired networks for intelligent structures," *Structural Health Monitoring*, 13(6):609–620, doi:10.1177/0725513614554076.
3. Zhuang, Y., F. Kopsaftopoulos, R. Dugnani, and F.-K. Chang. 2018. "Integrity monitoring of adhesively bonded joints via an electromechanical impedance-based approach," *Structural Health Monitoring*, 17(5):1031–1045, doi:10.1177/1475921717732331, invited paper.
4. Ferreira, P. M., M. A. Machado, M. S. Carvalho, and C. Vidal. 2022. "Embedded Sensors for Structural Health Monitoring: Methodologies and Applications Review," *Sensors*, 22(21):8320, doi:10.3390/s22218320.
5. Ramanathan, A. K., M. B. Gingerich, L. M. Headings, and M. J. Dapino. 2022. "Metal structures embedded with piezoelectric PVDF sensors using ultrasonic additive manufacturing," *Manufacturing Letters*, 31:96–100, ISSN 2213-8463, doi:https://doi.org/10.1016/j.mfglet.2021.08.001.
6. Ju, M., Z. Dou, J.-W. Li, X. Qiu, B. Shen, D. Zhang, F.-Z. Yao, W. Gong, and K. Wang. 2023. "Piezoelectric Materials and Sensors for Structural Health Monitoring: Fundamental Aspects, Current Status, and Future Perspectives," *Sensors*, 23(1), ISSN 1424-8220, doi:10.3390/s23010543.
7. Baptista, F. G., D. E. Budoya, V. A. D. d. Almeida, and J. A. C. Ulson. 2014. "An Experimental Study on the Effect of Temperature on Piezoelectric Sensors for Impedance-Based Structural Health Monitoring," *Sensors*, 14(1):1208–1227, ISSN 1424-8220, doi:10.3390/s140101208.
8. Ferreira, P. M., M. A. Machado, M. S. Carvalho, P. Vilaça, G. Sorger, J. V. Pinto, J. Deuermeier, and C. Vidal. 2023. "Self-sensing metallic material based on PZT particles produced by friction stir processing envisaging structural health monitoring applications," *Materials Characterization*, 205:113371.
9. Dziendzikowski, M., A. Kurnyta, K. Dragan, S. Klysz, and A. Leski. 2016. "In situ Barely Visible Impact Damage detection and localization for composite structures using surface mounted and embedded PZT transducers: A comparative study," *Mechanical Systems and Signal Processing*, 78:91–106, ISSN 0888-3270, doi:https://doi.org/10.1016/j.ymssp.2015.09.021, special Issue on Piezoelectric Technologies.
10. He, H., C.-l. Lu, J. Ren, J. Dhar, G. Saunders, J. Wason, J. Samuel, A. Julius, and J. T. Wen. 2025. "Open-source software architecture for multi-robot Wire Arc Additive Manufacturing (WAAM)," *Applications in Engineering Science*, 22:100204.
11. Akin, S., S. Lee, S. Jo, D. G. Ruzgar, K. Subramaniam, J.-T. Tsai, and M. B.-G. Jun. 2022. "Cold spray-based rapid and scalable production of printed flexible electronics," *Additive Manufacturing*, 60:103244.
12. Janapati, V., F. Kopsaftopoulos, F. Li, S. Lee, and F.-K. Chang. 2016. "Damage detection sensitivity characterization of acousto-ultrasound-based SHM techniques," *Structural Health Monitoring*, 15(2):143–161, doi:10.1177/1475921715627490.